Effects of Radial Distortion on Low-Speed Tandem Stage Axial Compressor

Hitesh T. Chhugani, Amit Kumar, and A. M. Pradeep

Abstract Aero-engine compressor designers have a challenging task of developing compressors that have a higher-pressure ratio and better efficiency with a lower number of stages. Such designs would require blades with high diffusion factor and hence the inherent risk of flow separation. Tandem blade is an interesting concept, which possibly addresses this problem. In tandem blading, the forward blade and the aft blades are arranged in such a manner that a converging nozzle flow path is created between the two blades. The flow accelerates through this nozzle, energizes the suction surface flow, and thereby prevents the early onset of flow separation. This paper presents the steady computational analysis of a tandem rotor stage and baseline stage in low-speed axial flow compressor at design and off-design condition using ANSYS CFX. The study is further extended to analyze the effect of radial distortion on the performance of tandem rotor and the single rotor.

Nomenclature

AA	Aft airfoil
AB	Aft blade
AO	Axial overlap
C_a	Axial velocity
C_{FA}	Chord of the forward airfoil
C_{FB}	Chord of the forward blade
DR	Degree of reaction
DF	Diffusion factor
FA	Forward airfoil
FB	Forward blade

H. T. Chhugani (✉) · A. Kumar · A. M. Pradeep
Indian Institute of Technology Bombay, Mumbai 400076, Maharashtra, India
e-mail: hiteshchhugani1@gmail.com

A. M. Pradeep
e-mail: ampradeep@aero.iitb.ac.in

G. Sivaramakrishna et al. (eds.), *Proceedings of the National Aerospace Propulsion Conference*, Lecture Notes in Mechanical Engineering,
https://doi.org/10.1007/978-981-19-2378-4_4

D	Lieblein diffusion factor
PP	Percentage pitch
PS	Pressure surface [Pa]
P_{ST}	Static pressure [Pa]
SS	Suction surface
TLV	Tip leakage vortex
U_{mid}	Tangential speed at rotor mean section
P_0	Total pressure [Pa]
R/H	Span percentage
Q	Q-Criterion
S	Shear strain rate
Cp	Static Pressure rise Coefficient $= \frac{P_{\mathrm{ST}} - P_{\mathrm{ST\_Inlet}}}{P_{\mathrm{O\_INLET}} - P_{\mathrm{ST\_INLET}}}$

Greek Symbols

α_2	Absolute air angle at the exit of conventional rotor
Θ_{AA}	Aft airfoil Camber
K	Airfoil blade angle relative to axial coordinate
Θ	Camber angle
ρ	Density
ϕ	Flow coefficient $= \frac{Ca}{U_{\mathrm{mid}}}$
Θ_{FA}	Forward airfoil Camber
η	Isentropic Efficiency
Θ_{OV}	Overall Camber
Ψ	Stagnation Pressure Loss coefficient $= \frac{P_{\mathrm{O\_LE}} - P_{\mathrm{O\_TE}}}{\frac{1}{2} * \rho * U_{\mathrm{mid}}^2}$
ω	Total pressure loss coefficient $= \frac{P_{\mathrm{O\_LE}} - P_{\mathrm{O\_TE}}}{P_{\mathrm{O\_INLET}} - P_{\mathrm{ST\_INLET}}}$

Subscripts

11	Forward airfoil/blade at inlet
12	Forward airfoil/blade at exit
21	Aft airfoil/blade at inlet
22	Aft airfoil/blade at exit

1 Introduction

The compressor is a major part of an aeroengine, which acquire large portion, and it largely affects the performance of an aero engine. Future demands of smaller,

lighter, and more efficient aeroengines can be achieved by evolving compressors design. This can be done by designing a stage that can achieve a higher-pressure rise without affecting the overall efficiency. In the compressor, flow separation restricts the upper limit of pressure rise per stage. Several studies in the past were focused on controlling the boundary layer to achieve a higher total pressure ratio per stage. Such studies include slotted blades, boundary layer suction, and boundary layer blowing and tandem blading. However, very few of those have been implemented by industries in the compressor rotor owing to the nature of the operation and mechanical difficulties involved.

Such studies include slotted blades, boundary layer suction, and boundary layer blowing and tandem blading. However, very few of those have been implemented by industries in the compressor rotor owing to the nature of the operation and mechanical difficulties involved. In recent years, researchers have drawn lot of interest in Tandem blading. Tandem blade is a set of two blades, one is forward blade and second is an aft blade. Figure 1 shows the schematic configuration of Tandem Blade.

There are two important defined parameters, which fix the position of the aft blade with respect to the forward blade. Firstly, axial overlap (AO) determines the axial position of the aft blade, with positive overlap; aft blade will come closer to the forward blade. While the tangential position of the aft blade can be altered by varying the percentage pitch (PP), the axial overlap and the percentage pitch are defined as follows:

$$\mathrm{AO} = \frac{\Delta L}{L} \tag{1}$$

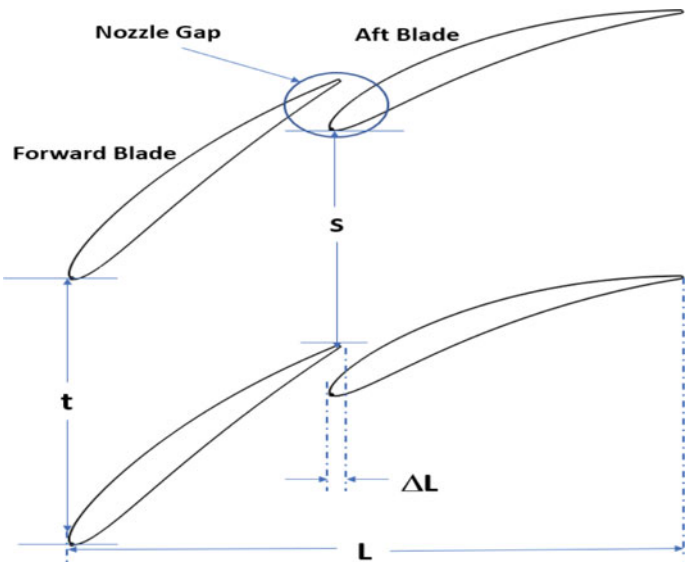

Fig. 1 Schematic of tandem blade

$$\mathrm{PP} = \frac{\mathbf{s}}{\mathbf{t}} \tag{2}$$

This forward blade and aft blade are positioned in such a way that it forms a gap between them, which act as a nozzle for the flow coming from pressure surface of the forward blade. This region between FB and AB is termed as a gap nozzle. As flow passes through this region, it gets accelerated and thus it provides additional momentum to flow that prevents flow separation over the suction surface of the aft blade. Hence, this mechanism allows the compressor designer to design a compressor blade with higher flow turning angle, thus achieving higher-pressure rise per stage is possible by using tandem balding configuration. The exit angle of the forward blade is considered as inlet angle for the aft blade while designing the tandem rotor. FB is supposed to operate as a conventional rotor; however, flow over AB is well controlled by FB in design and off-design condition. Many researchers have conducted their experimental and computational investigation in past also.

Roy and Saha [1] carried out low-speed studies to find the diffusion capability of the tandem cascade (CDA 21–21) and compared it deflection capability with CDA 43 (single airfoil) with CDA 21–21 (tandem). Experimental studies over CDA 43 and CDA 21–21 (single and tandem cascade) showed that CDA 21–21 (tandem cascade) can have higher deflection capability but their operating range is very less. Falla [2] computational study on a tandem airfoil with NACA-65, reported that a tandem configuration with low AO and high PP is suitable for tandem configuration. Various key points were emerged out of the work conducted on 2D-Tandem Airfoils. PP and AO play have a first order effect on the performance of tandem airfoil. Higher PP and lower AO were able to achieve the best performance. Loading distribution between forward and aft blade affect the performance of tandem airfoil. McGlumphy et al. [3, 4] did a computational analysis in a subsonic region of NASA 65 tandem airfoil. Performance analysis was done for different combination, i.e., by changing Axial Overlap and Percentage Pitch. Along with that, the effect of blade loading split between AB and FB on overall performance was studied, for different PP and AO. Based on aerodynamic parameters and the mechanical limitations, the optimum design of Tandem blade was chosen with 85% PP and 0 AO. Hasegawa et al. [5] carried out a test on single stage transonic compressor in which tandem rotor and single blade stator were used along with outlet guide vanes, effectively making stator as the tandem blade. Linnemann [6] conducted a series of test at low speed on blower which has both tandem stator and rotor. To determine optimum configuration, the position of the tandem blade was varied. The conclusion from various test came out as tandem airfoil with 0 AO and 80% PP can give maximum pressure rise and maximum efficiency for both rotor and stator. Brent and Clemmons [7] carried out experiments over two different tandem rotors and single blade rotor. The two tandem rotors used were having different load split of 50–50 and 20–80 on forward and aft blade. In the case of 20–80 load split, more losses were observed in comparison with 50–50 load split. Bammert and Staude [8] carried out experimentation and tested tandem rotor in a 5-stage compressor. Out of 5 stages, middle 3 stages consist of a tandem rotor. Similarly, the low operating range was observed and also was able to achieve

higher loading because of tandem rotors. GE J-79 compressor and an advanced single stage LP compressor built by Honeywell (2005) are some examples of commercial turbomachinery where tandem blades are employed as stators. Weber and Steinert [9] carried out CFD and experimental investigation on a transonic tandem compressor cascade which was designed for high flow turning. The total pressure loss coefficient reported was 0.15.

The compressor is designed with the assumption of clean inlet flow. The inlet flow condition can severally affect the performance of the aircraft compressor. In actual scenario, the flow at engine inlet is generally distorted. The extent of distortion depends on engines application and its size. Engine encounters non-uniformity in the inlet flow during maneuvers, ingestion of foreign objects, and crosswinds. Similar to the tandem case, results of the lower operating range are observed in aero engine with the non-uniform flow at inlet. There are various experimental and computational work which have analyzed flow physics in the conventional compressor under distorted inflow conditions. Lee et al. [10, 11] observes considerable loss in overall performance and stability of the engine together along with that increase Specific Fuel Consumption and drop in engine thrust was observed. Numerical investigation of inlet distortion due to crosswind effects for high bypass ratio turbofan engine was done by Liu et al. [12]. In experimental and computational studies, special screens are used to replicate the different inflow distortion conditions. These screens are mounted upstream of the compressor. In the future's engine concept like BLI engines (2014), the boundary layer developed over fuselage is ingested into the intake of engines. Therefore, from a future perspective, it is important to understand the effect of distorted inlet flow on the overall performance of a compressor with highly loaded tandem blades. This knowledge can be helpful in designing a compressor with tandem blades. Researches carried out were more related to tandem stator and cascade which concluded higher diffusion factor for tandem cases. Kumar and Pradeep [13] study the performance and feasibility of the tandem rotor when used with a single rotor. The better performance was observed in comparison with a conventional rotor at the design point. The present computational study compares the performance of a stage with the conventional rotor and with the tandem rotor under clean and radially distorted inflow condition. The effect of the tandem rotor and conventional rotor on the single stator is also analyzed. The paper also analyzes the effect of the tandem blade on tip leakage flow and how the tip leakage is affected under radially distorted inflow condition. The main goal of this study is to understand the effect of the radial hub and tip distortion on tandem blade rotor stage. The study can be useful in the future to for the optimization of the tandem blade rotor stage. If the tandem blades are used in commercial turbomachinery, we will have a comparatively smaller size engine as it will bring down the number of compressor stages.

2 CFD Validation

The validation of computational results is done with experimental results of baseline stage. Experimental results on baseline stage are referred from Kumar and Pradeep [13]. Table 1 show blade design parameters of the baseline stage. ANSYS CFX is used for steady RANS computational analysis. The domain length of the inlet is 1.5 chord upstream of rotor trailing edge while the domain length of outlet is 2.5 chord downstream of stator trailing edge. The structured mesh is generated using ANSYS Turbogrid through Automatic Topology and Meshing (ATM) method. Mesh generated around the rotor and stator blade is O-Grid while the mesh generated in the passage is H-Grid with the width factor of 0.5. For Near wall, design specification in case of both baseline rotor and stator y+ method is used. In the case of the rotor, the constant tip gap of 1 mm is maintained. Before validating the results with experimental data, the grid-independent study is performed to determine grid-independent mesh. The parameters used to see grid independency is isentropic efficiency. The solution is called grid-independent when a change in isentropic efficiency is ± 0.5 to 1%.

Figure 2a shows the grid independence study of baseline stage with the help of isentropic efficiency. In the case of baseline rotor stage, grid independency solution is obtained for the number of elements equal to 1.5 million. ANSYS-CFX Pre is used to apply boundary conditions and turbulence model and set the convergence criteria. The turbulence model used for computational analysis is SST K-ω. This model is preferred for analysis, as its results match well with experimental results. Turbulence intensity selected for simulation is 5%. The total pressure of 101325 Pa and total temperature of 300 K are defined as the inlet boundary condition. The mass flow rate is used as an outlet boundary condition. The RPM of the rotor is set to 2700. Convergence criteria is set to be achieved when RMS residual is below 10^{-6}. Isentropic efficiency and mass imbalance are two other monitors to check the convergence of the solution.

Figure 2b shows the comparison of experimental results and computational results of the baseline stage. CFD results show good agreement with the experimental data.

Table 1 **a** Design parameters of the single rotor (2019) **b** design parameters of the stator of the baseline stage (2019)

a			
Baseline rotor	Tip	Mean	Hub
DF	0.50	0.54	0.47
DR	0.78	0.70	0.50
Camber angle (°)	23.0	35.0	60.0
b			
Baseline stator	Tip	Mean	Hub
DF	0.53	0.48	0.45
Camber angle (°)	50.0	50.0	52.0

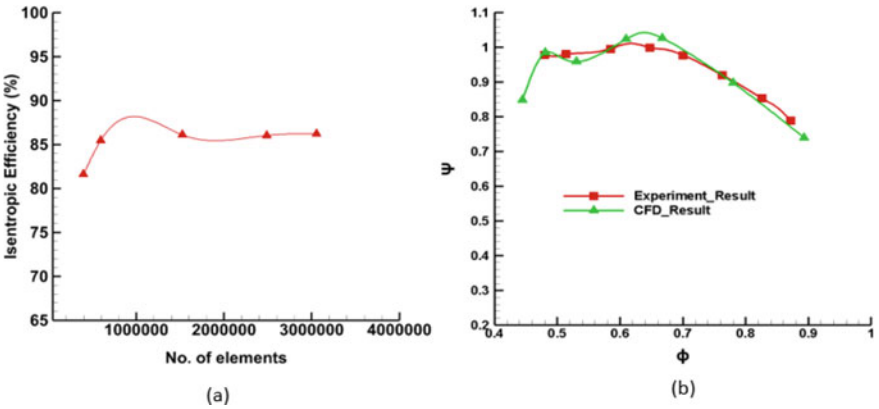

Fig. 2 **a** Grid independence of baseline stage **b** experimental validation of CFD result of baseline stage

With CFD validation, further computational analysis of the tandem stage is carried out under different inflow conditions.

3 Design of Tandem Rotor Stage

The combination of tandem rotor and the single stator is referred as a tandem stage in this paper (Table 2), whereas the baseline stage is consisting of a single rotor and single stator (Table 1). In the design of a tandem rotor, a higher-pressure rise is attempted by increasing the flow turning angle. Both the tandem rotor and the single rotor are designed with 2700 RPM. The designed mass flow rate for both the stages, i.e., baseline stage (single rotor and single stator) and tandem stage is 6 kg/s. Based

Table 2 **a** Design specifications of the tandem rotor (2019) **b** design parameters of the stator of the baseline stage (2019)

a

Tandem rotor	Forward blade			Aft blade		
	Tip	Mean	Hub	Tip	Mean	Hub
DF	0.44	0.46	0.44	0.52	0.49	0.31
Camber angle	16.5°	20.6°	30.9°	26.1°	35.3°	42.6°
Stagger	57.5°	46.4°	28.1°	45.1°	26.6°	0.86°

b

Baseline Stator	Tip	Mean	Hub
DF	0.53	0.48	0.45
Camber Angle	50.0°	50.0°	52.0°

on the past literatures, a higher PP and low AO (5AO and 85PP) is selected for the computational analysis. The blade loading is equally split between the forward and the aft rotor. Owing to the low-speed application, C4 blade profile is used for the designing of rotor and stator in both stages. The chord length of the baseline stage rotor is equal to sum of chord length of AB and FB. A total number of 19 forward rotor blades and 19 aft rotor blades are used in tandem stage design, whereas 19 single rotor blades are used in the baseline stage. In both stages, 21 numbers of single stator blades are used.

ANSYS CFX is used for steady RANS computational analysis. The domain length of inlet is 1.5 chord upstream of rotor trailing edge, while the outlet is positioned at 2.5 chord downstream of stator trailing edge. As ATM failed to generate good quality of mesh in case of the tandem rotor, traditional control point method is used to generate the mesh in the tandem rotor domain. The overall skewness of 18° achieved in tandem rotor domain. H-Grid is formed in Inlet and outlet domain, while O-grid is formed around blade surface. The width factor in case of a stator with the tandem rotor is set to 0.5. For Near wall, design specification in case of both tandem rotor and stator y+ method is used.

Figure 3 shows the grid independence of the tandem rotor stage. The isentropic efficiency is almost constant after 2.82 million nodes; therefore, 2.82 million nodes are finalized for the computational analysis. The boundary condition, turbulence model, turbulence intensity, and convergence criteria in tandem rotor stage are similar as of baseline stage. In the case of the tandem rotor, constant tip gap of 1 mm is maintained.

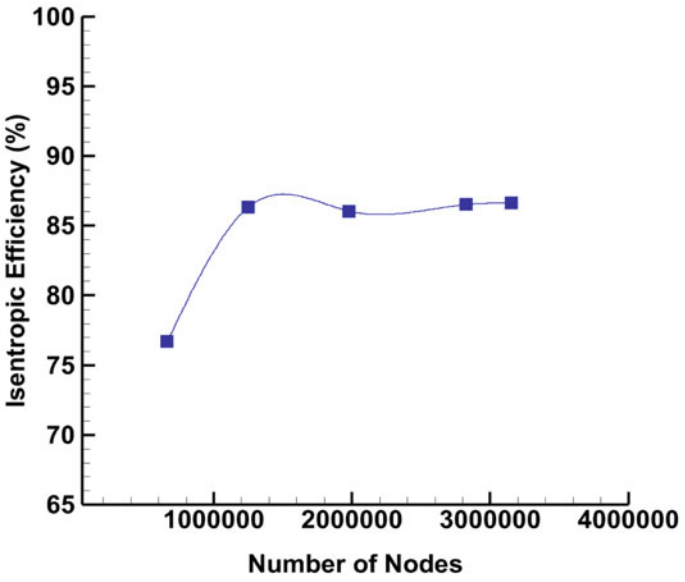

Fig. 3 Grid independence of tandem rotor stage

4 Results and Discussion

The computational results for tandem rotor stage and baseline stage are analyzed at design and off-design condition for different inflow condition. Figure 4 shows the total pressure profile of clean flow, radially hub distorted and radially tip distorted flow at inlet. The radial distortion flow is created using the distortion screen, which is positioned 400 mm upstream of the rotor leading edge. The boundary layer profile of radial hub distortion and radial tip distortion are extracted with the help of the 7-hole probe, which is traversed at 1.5 chord upstream of rotor LE.

4.1 Clean Flow

(1) Mach contour, embedded with streamline, are plotted at a different percentage of blade span, i.e., 10, 50, and 90% for tandem rotor stage and baseline stage at. Figures 5a and 6a show the Mach contours for tandem rotor stage at design mass flow rate, i.e., $\varphi = 0.64$ and off-design condition, i.e., $\varphi = 0.534$. Similarly, Fig. 5a, b show the Mach contours at the different percent of blade span for baseline stage under design ($\varphi = 0.64$) and off-design condition ($\varphi = 0.534$). In Fig. 6a, at 10% span, small flow reversal is observed near the trailing edge of the aft blade at design mass flow rate.

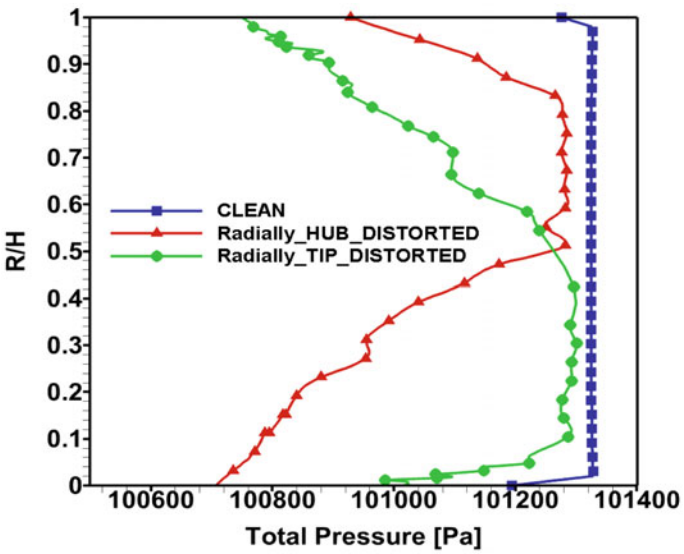

Fig. 4 Total pressure profile at inlet

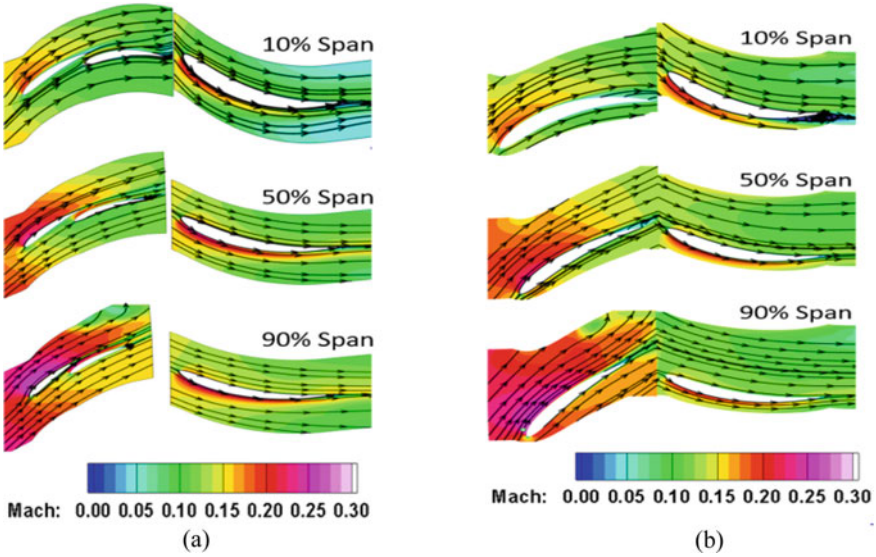

Fig. 5 **a** Mach contour of tandem rotor stage at $\varphi = 0.64$ under clean inlet flow condition **b** Mach contour of baseline stage at $\varphi = 0.64$ under clean inlet flow condition

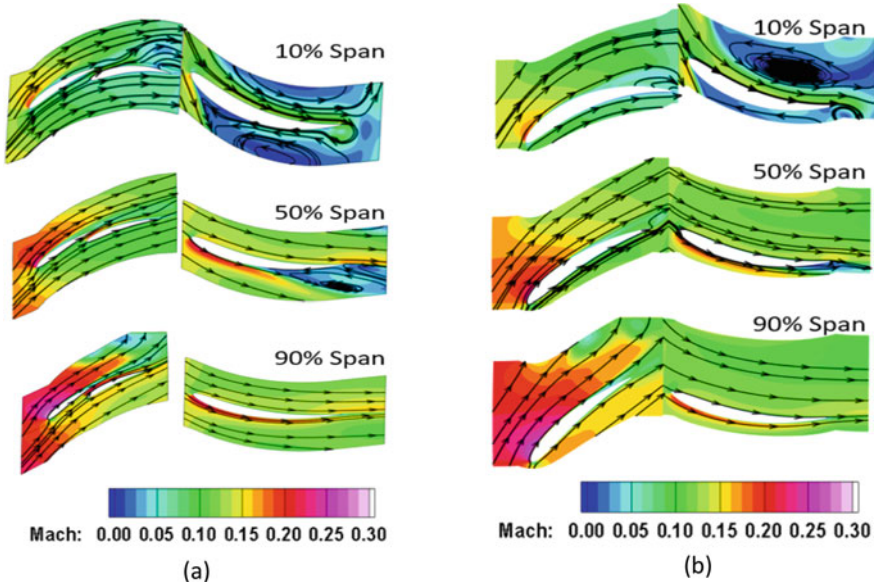

Fig. 6 **a** Mach contour of tandem rotor stage at $\varphi = 0.534$ under clean inlet flow condition **b** Mach contour of baseline stage at $\varphi = 0.534$ under clean inlet flow condition

At higher span, as the effectiveness of the tandem blading increases, flow separation gets attenuated and both tandem rotor blades operate more efficiently (50 and 90% span in Fig. 5a). The Mach number increases from hub to tip region in both baseline and Tandem stage. At 10% span of tandem stage, flow separation region over aft blade SS enlarges further (Fig. 5b). In the comparison of the tandem rotor, baseline rotor is free from flow reversal under design point; however, lower blade Sect. (10 and 50% span in Fig. 6b) shows a significant deviation in streamlines under off-design condition. The stator of the tandem stage is designed with higher flow turning angle, lower energy with higher incidence lead to huge flow reversal over stator blade suction surface at lower span (Fig. 6a). Similar nature of flow is also visible over the stator of the baseline stage, where 90% of the blade portion is covered with the reverse flow (Fig. 6b).

Losses occur in the tip region accounts for the one-third of overall losses in turbomachinery. Therefore, it is imperative to analyze the new design for tip leakage losses. The tip leakage behavior is compared under the design and the off-design condition. When the tip leakage flow meet with the mainstream flow in a passage between the rotor blades, it rolls up into Tip leakage vortex (TLV) near the suction side of the blade. TLV is presented with the help of Q-Criterion, which represents the local balance between the magnitude of vorticity (Ω) and shear strain rate (S) in Fig. 7a, b. In case of a tandem rotor (Fig. 7a), two strong TLV are observed one from FB and another from AB. The trajectory of TLV depends upon the axial momentum of the mainstream flow and tangential momentum of Tip leakage flow. In case of the tandem blade, the loading is divided among the FB and AB; therefore, the strength of each TLV is weaker than TLV from baseline rotor blade. Strength of the TLV of the forward blade is significantly higher than TLV of the aft blade. Further, The TLV from AB interacts with the flow coming from the nozzle gap. Tip leakage vortex of the aft blade is appeared to be more aligned axially after the interaction with

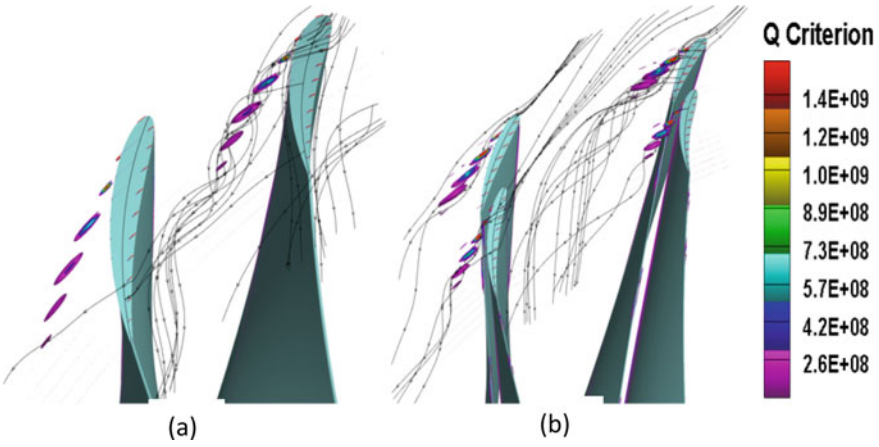

Fig. 7 Q-Criterion plot for **a** baseline rotor **b** tandem rotor at $\varphi = 0.64$ under clean inlet flow condition

gap-nozzle flow. Under design condition, the streamlines from FB-TLV are directed toward the LE of adjacent AB. While in case of baseline rotor blade, it is directed toward TE of the adjacent blade. As the PP of the tandem blade is higher, i.e., 85%, therefore, wake from FB interacts with the AB-TLV and decelerate the AB-TLV in that region.

To further signify the blockage created due to TLV, Mach number contours are drawn at 95 and 98% blade span and shown in Fig. 8a, b. Blockage at 98% span is substantially higher than the blockage at 95% span, as strength of TLV is higher near the tip. In case of the tandem rotor, owing to stronger tip leakage vortex, significantly higher flow blockage is observed near 98% span. FB-TLV and AB-TLV merges downstream and forms a large flow blockage in this region. The blockage region in the single rotor is lower than the tandem rotor blockage. However, other than TLV, a scrapping vortex is visible near the trailing edge of the single blade; however, the strength of the scrapping vortex is considerably lower than TLV. Unlike the tandem rotor, TLV and scrapping vortex moves separately without any evidence of immediate mixing.

Under the off-design condition, Q-Criterion is plotted near tip region at near stall condition for baseline and tandem rotor in Fig. 9a, b, respectively. At near stall condition, the tip leakage vortex enlarges in comparison with TLV at the design condition. Near the stall condition, the momentum of mainstream flow is lower. Therefore, the tangential momentum dominates over the axial momentum of the flow. For the baseline rotor, TLV is directed toward the mid-chord of the baseline rotor blade. On the contrary, TLV was directed toward trailing edge under design condition. Similarly, in case of a tandem rotor blade, FB-TLV is affecting the TE of the FB of the adjacent tandem blade near stall condition. The AB-TLV makes a higher angle with the axial flow direction. The strength of AB-TLV decreases due to reduced tip loading near the stall point.

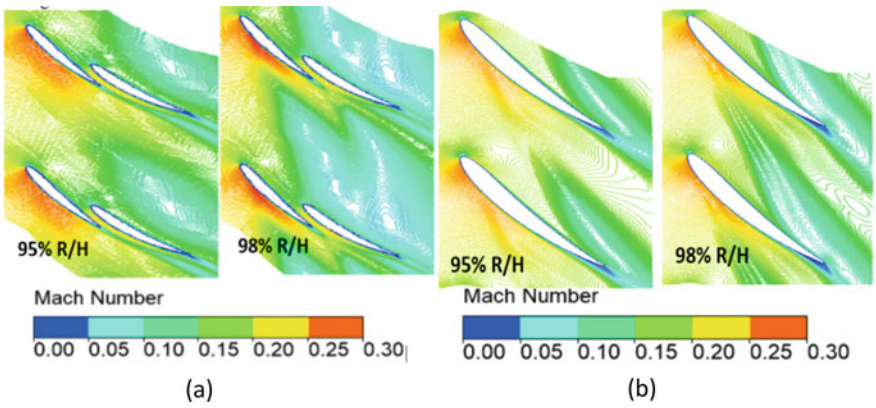

Fig. 8 Mach contour at 95 and 98% span of **a** tandem rotor blade span **b** baseline rotor blade at $\varphi = 0.64$

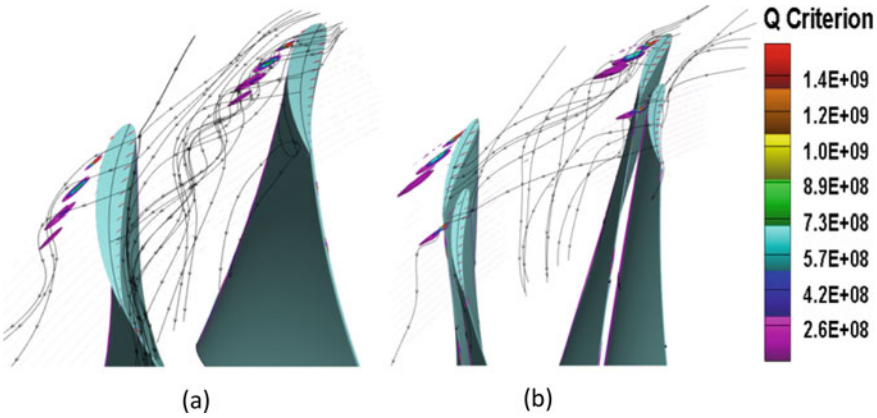

Fig. 9 Q-Criterion plot for **a** baseline rotor **b** tandem rotor at $\varphi = 0.534$ under clean inlet flow condition

Figure 10a, b show the Mach contour plot at 98 and 95% of baseline and tandem rotor blade span, respectively, at near stall condition. For both rotors, the blockage region increases significantly near the stall point. Further, for the baseline rotor, the trajectory of TLV changes and it is directed toward the mid-chord section of the blade, which is different from what was observed under design point. The flow blockage due to scrapping vortex is increased near stall condition. Near stall condition, the scrapping vortex is observed at lower chord length in comparison with what is observed at the design condition. Due to higher tangential momentum of scrapping vortex, TLV and scrapping vortex interacts and forms a bigger blockage region.

Similarly, in case of a tandem rotor blade, the flow blockage due to TLV increases at near stall condition (Fig. 10a) in comparison with design condition. Even at 95% of blade span, significant blockage region is observed. At near stall condition, a small

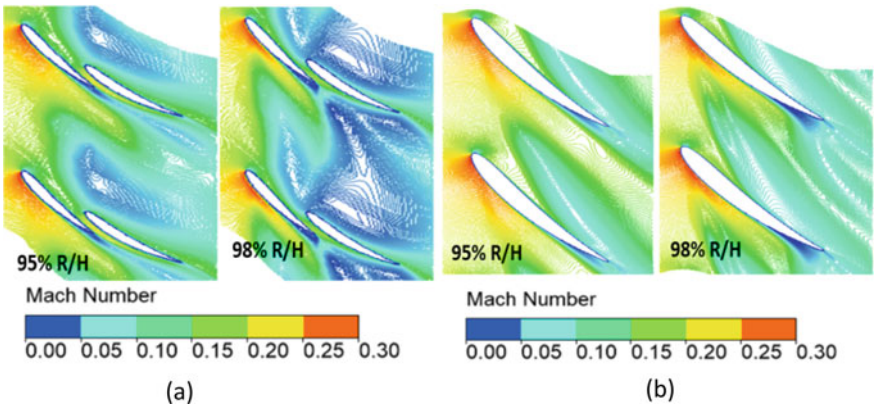

Fig. 10 Mach contour at 95 and 98% of **a** tandem rotor **b** baseline rotor blade span at $\varphi = 0.534$

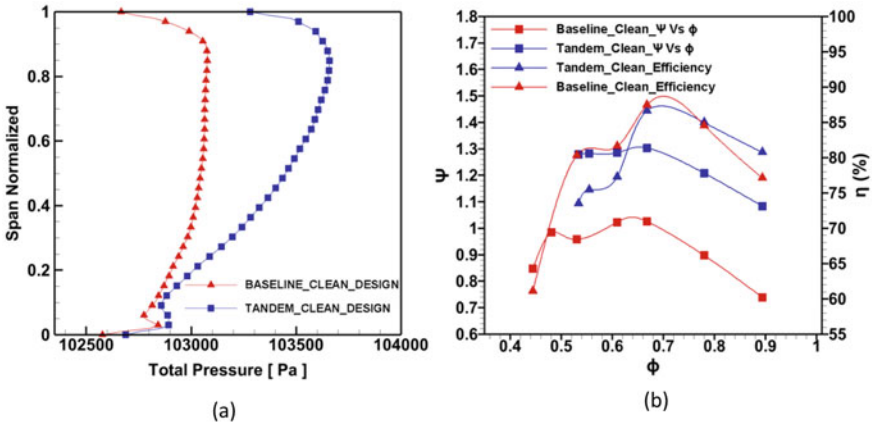

Fig. 11 **a** Total pressure across the blade span at $\varphi = 0.64$ **b** isentropic efficiency and total pressure rise coefficient versus flow coefficient (φ) under clean inlet flow condition

amount of flow blockage is also observed near trailing edge of FB, which is due to FB wake. At 98% span, blockage region further enlarges. Other than FB-TLV and AB-TLV, wake emanating from FB and AB also contributes to the blockage region. All vortices combine and make a larger flow blockage region near tip in comparison with baseline rotor.

Figure 11a shows the spanwise profile of total pressure at the exit of a stator for the tandem rotor stage and baseline stage under design condition. It is observed that throughout the blade span pressure rise is higher in case of tandem rotor stage. Design of tandem rotor is such that the pressure rise is higher near tip compare to the hub region.

Figure 11b shows the comparison of isentropic efficiency for tandem rotor stage and baseline stage. At a higher mass flow rate, the adiabatic efficiency of the tandem stage is marginally higher than the baseline stage. However, at the lower mass flow rate, a significant drop in adiabatic efficiency of the tandem rotor is observed. The large drop in efficiency for the tandem stage is largely attributed to huge flow separation over the stator suction surface. Other than this, losses associated with TLV are significantly increased near the stall point, which results in a further drop in adiabatic efficiency. Figure 19 compares the performance map of the baseline stage and a tandem stage. At the design mass flow rate, the tandem stage demonstrates an increment of around 26.58% in total pressure than the baseline stage. The drop in a stall range is observed for the tandem rotor stage. The tandem rotor stage has a stall margin of 20%, which is 13% lower than the stall margin of the baseline stage.

4.2 Radial Hub Distortion

The performance of the tandem stage and the single stage under radial hub distortion is compared in this section of the paper. Mach contour is plotted at 10, 50, and 90% of blade span for baseline and tandem rotor stage at design condition, i.e., $\varphi = 0.64$. At 10% of blade span, the flow coming from nozzle gap detached from around mid-chord of the SS of AB. This is mainly because of distorted flow near the hub region and lower effectiveness of the nozzle gap. The flow looks like what was observed under clean flow inlet condition at near stall condition. Due to cumulative effect of higher flow turning angle, higher incidence, a low hub to tip ratio, and considerable boundary layer growth at lower span, huge flow separation is observed over stator suction surface even at design mass flow rate.

In the case of the baseline rotor (Fig. 12b), flow shows a significant deviation of around 75% of the blade chord. Like the previous case of the tandem stage, 90% stator suction surface is covered with the reverse flow. However, the vortex core is shifted toward the trailing edge of the stator in the baseline stage. At higher span, tandem stage exhibits the improved performance. Improved performance at higher span is mainly attributed to a reduction in inlet distortion level, increase in nozzle gap effectiveness, and lower camber angle of the blade. At 50% span, small flow separation is visible at the trailing edge of the stator suction surface of the tandem stage (Fig. 12a). On the contrary, at higher span, flow adhere to the blade profile in the case of the baseline stage.

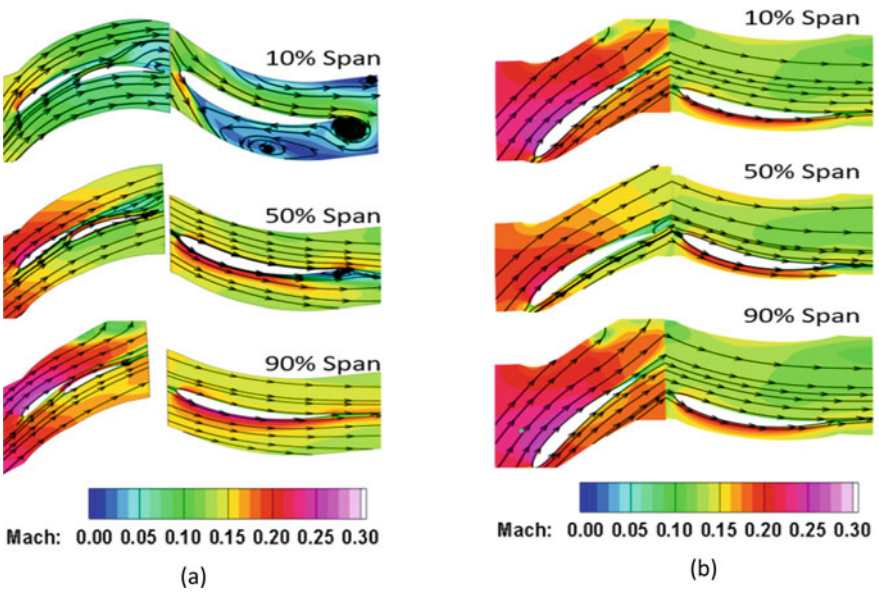

Fig. 12 Mach contour of **a** tandem rotor stage **b** baseline rotor stage at $\varphi = 0.64$ under radial hub distorted inlet flow condition

Figure 13a, b shows the Q-Criterion plot near tip region of baseline rotor and tandem rotor, respectively, at design condition, i.e., at $\varphi = 0.64$. In the case of hub distortion, the mass flow rate near the tip region is higher in comparison with clean inlet flow condition. The AB seems so more loaded near the tip region under hub distortion case. Therefore, the intensity of AB-TLV is slightly higher in hub distortion case. Interestingly, FB in the tandem rotor and baseline rotor appears to be slightly less loaded in hub distortion case.

Thus, TLV from FB in the tandem rotor and baseline rotor is slightly weaker in hub distortion case. Due to the higher mass flow rate near the tip region, TLV is slightly more oriented in the axial direction in comparison with what is seen in clean flow. AB-TLV is also more directed in a streamwise direction in comparison with what is observed in clean flow. The blockage region due to TLV is further signified with the help of Mach number contours at 95 and 98% span is shown in Fig. 14a, b. Due to higher mass flow toward the tip region, the flow blockage is observed somewhat lower in case of hub distortion case in comparison with clean inlet flow condition.

Figure 15a shows the total pressure along the blade span of baseline stage and tandem rotor stage at $\varphi = 0.64$. The total pressure rise for the tandem stage is highly distorted. Interestingly, at blade section lower than the mid-span, the baseline stage demonstrates marginally higher total pressure rise than the tandem rotor. Thereafter, the tandem stage has a significantly higher total pressure rise than the baseline stage.

Figure 15b shows the comparison of isentropic efficiency for tandem rotor stage and baseline stage. At the design point, the baseline stage has around 4% higher isentropic than the tandem rotor stage. Figure 15b shows the performance map of the baseline stage and a tandem stage. At the design mass flow rate, the tandem stage demonstrates an increment of around 31.89% in total pressure than the baseline stage. In comparison with a clean flow drop of around 6.5% is observed in the tandem rotor stage under radial hub distortion condition. Both stages experience a drop in stall

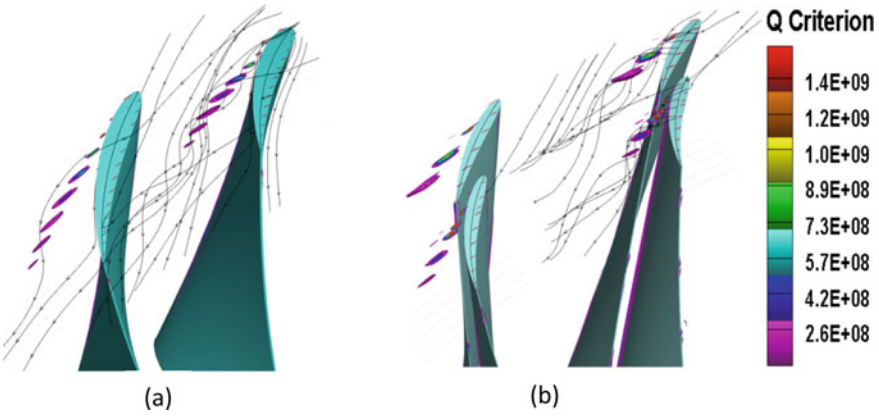

Fig. 13 Q-Criterion plot for **a** baseline rotor **b** tandem rotor at $\varphi = 0.64$ under radial hub distorted inlet flow condition

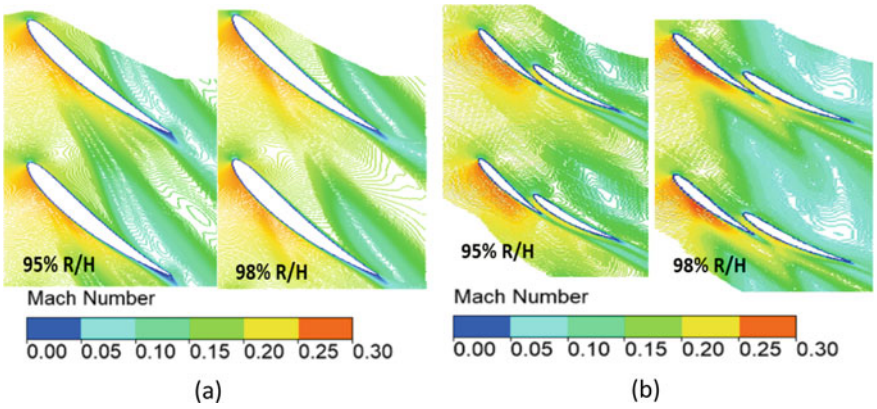

Fig. 14 Mach contour at 98 and 95% of blade span for **a** baseline rotor **b** tandem rotor at $\varphi = 0.64$ under radial hub distorted inlet flow condition

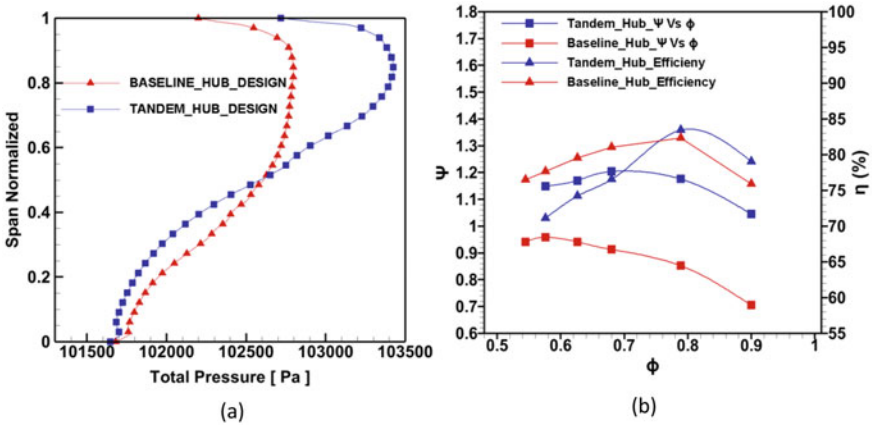

Fig. 15 **a** Spanwise total pressure profile at stator exit of baseline and tandem rotor stage at $\varphi = 0.64$ under radial hub distorted inlet flow condition **b** isentropic efficiency and total pressure rise coefficient versus flow coefficient (φ) under radial hub distortion inlet flow condition

margin under hub distorted flow. In comparison with the baseline stage, the tandem stage has 4% lower stall margin under hub distorted flow.

4.3 Radial Tip Distortion

The tip distorted profile used at the inlet of the computational domain is shown in Fig. 5. Mach contour is plotted at 10, 50, and 90% of blade span for baseline and tandem rotor stage at design condition in Fig. 16a, b. In case of a tip distortion, Mach

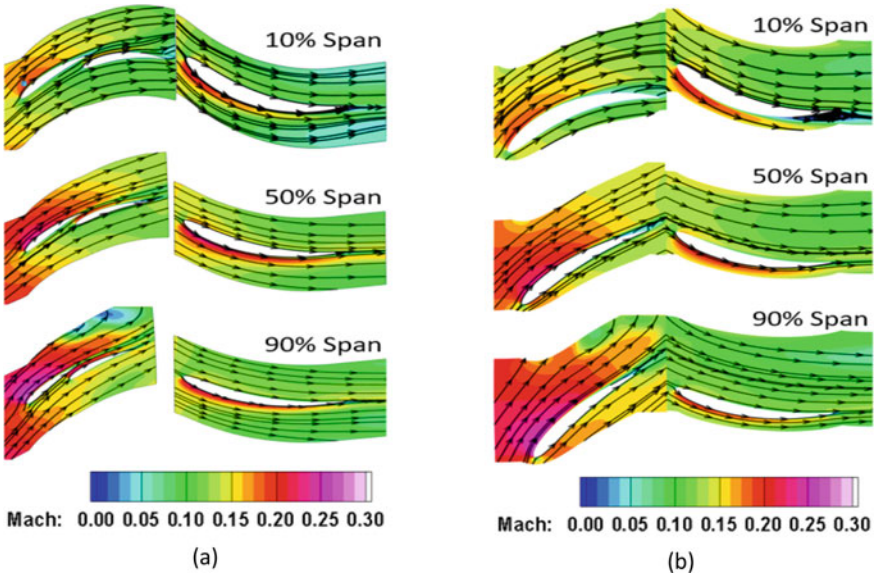

Fig. 16 Mach contour of **a** tandem stage **b** baseline stage at $\varphi = 0.64$ under radial tip distortion inlet flow condition

number at 10% of blade span is slightly higher than what is observed in case of clean flow. In Tandem rotor (Fig. 16a), low Mach number region is observed at 90% of span, mainly due to the reduced axial velocity near the tip region. In both baseline and Tandem rotor stage, the flow streamlines at 10, 50, and 90% of blade span look similar to what is observed in case of clean of flow.

Like previous cases, TLV under tip distortion is illustrated using Q-Criterion plot and streamlines in Fig. 17. As the flow is distorted near the tip region, a higher incidence results in a higher tip loading and consequently a stronger the tip leakage vortex. Due to the lower axial momentum of flow near the tip region, TLV has higher tangential momentum and TLV makes a higher angle to the axial flow direction. The flow physics near the tip region in both baseline and tandem rotor appear similar to what was observed under clean inlet flow condition near stall point. The streamlines show that in case of the baseline rotor, the TLV is directed toward the mid-chord of the adjacent blade. In case of the tandem rotor, the TLV from FB is directed toward the LE of AB of an adjacent tandem rotor blade. Similarly, as it is observed before, AB-TLV is weaker in comparison with the FB-TLV. In comparison with the baseline rotor, both TLV combines and results in a higher loss near the tip region.

Figure 18 show the Mach contour near the tip region at the design condition. At 98% of baseline rotor blade span, the TLV and scrapping vortex interact and create a large flow blockage region. This effect reduces at 95% of span. For the tandem rotor, a large area of flow blockage observed under tip distortion, even at design mass flow rate. There is an interaction of FB-TLV, AB-TLV, and wake from the FB lead to large flow blockage in comparison with what is observed in the case of baseline

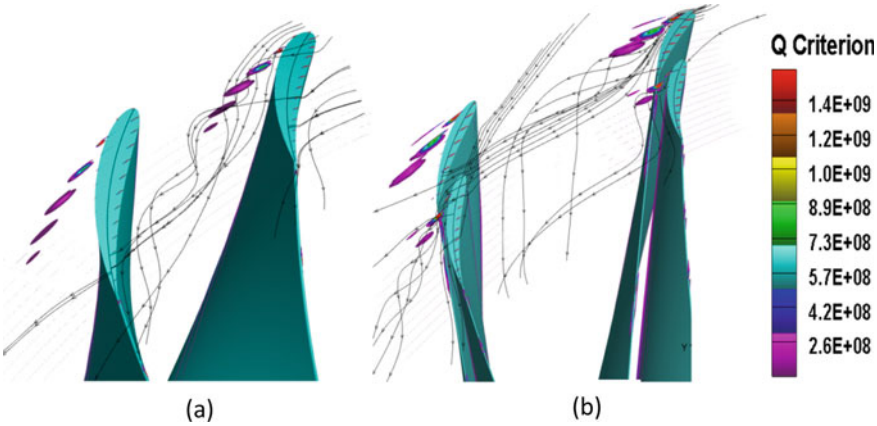

Fig. 17 Q-Criterion plot for **a** baseline rotor **b** tandem rotor at $\varphi = 0.64$ under radial tip distortion inlet flow condition

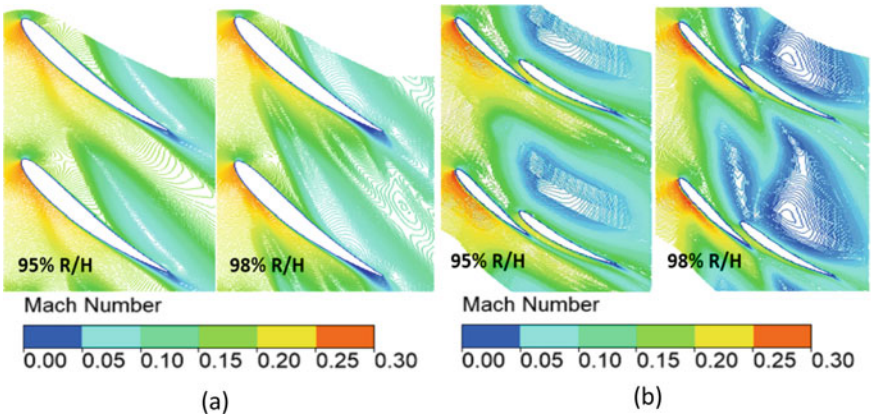

Fig. 18 Mach contour at 98 and 95% of **a** baseline rotor **b** tandem rotor at $\varphi = 0.64$ under radial tip distortion inlet flow condition

rotor. This large area of flow blockage near the tip region leads to the sudden stall of the tandem rotor stage. A significant blockage can be even seen at 95% of the blade span.

Due to the lower axial momentum of flow near the tip region, TLV has higher tangential momentum and TLV makes a higher angle to the axial flow direction. The flow physics near the tip region in both baseline and tandem rotor appear like what was observed under clean inlet flow condition near stall point. The streamlines show that in case of the baseline rotor, the TLV is directed toward the mid-chord of the adjacent blade. In case of the tandem rotor, the TLV from FB is directed toward the LE of AB of an adjacent tandem rotor blade. Similarly, as it is observed before,

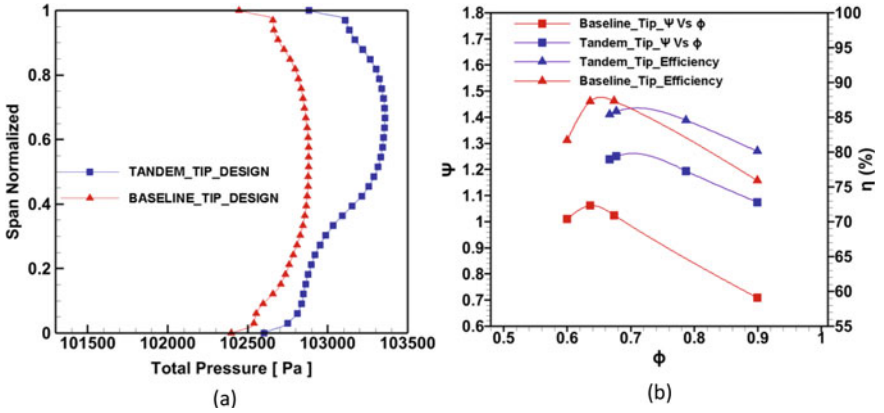

Fig. 19 **a** Spanwise total pressure profile at stator TE of tandem rotor stage and baseline stage at $\varphi = 0.64$ under radial tip distortion inlet flow condition **b** isentropic efficiency and total pressure rise coefficient (Ψ) versus flow coefficient (φ) under radial tip distortion inlet flow condition

AB-TLV is weaker in comparison with the FB-TLV. In comparison with the baseline rotor, both TLV combines and results in a higher loss near the tip region.

Figure 19a shows the total pressure profile at the exit of stator near the design point. Tandem rotor demonstrates higher-pressure rise throughout the span the baseline stage. Effect of the distorted tip region can be seen in the total pressure profile. After 75% of the blade span, the total pressure drops gradually toward the tip region. The difference in total pressure seems to be more significant at higher span.

Fig. 19b shows the comparison of isentropic efficiency for tandem rotor stage and baseline stage. At the design point, the baseline stage seems to have around 1.5% higher isentropic efficiency than tandem rotor stage. Figure 19b shows the performance map of the baseline stage and a tandem stage. At design condition, tandem rotor yields 22.12% higher-pressure rise in comparison with the baseline case under tip distortion. Tandem stage stall even before it reaches its design mass flow rate. The early stall under the tip distortion is attributed to higher incidence near the tip region and highly loaded tip design. A relax tip design could improve the stall margin of the tandem stage. The baseline stage has 10% higher stall margin in comparison of the tandem stage.

4.4 Tandem Rotor Stage

Figure 20a shows the spanwise variation of total pressure for the tandem stage under different inflow condition. The total pressure rise under clean flow is higher than the other cases. Pressure rise appears to be more affected under the hub distortion, where the highly distorted profile can be seen realized. The drop in total pressure can be noticed after 75% span under the tip distorted case.

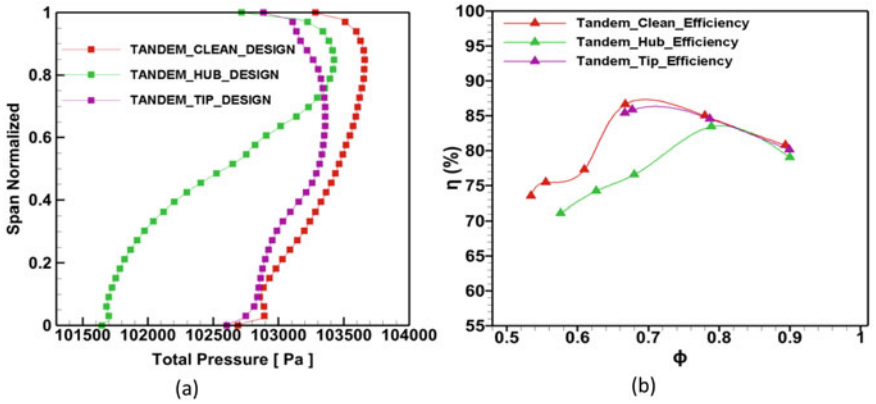

Fig. 20 **a** Spanwise total pressure profile at stator TE of tandem rotor stage at $\varphi = 0.64$ **b** isentropic efficiency for tandem rotor stage

Figure 20b compares the isentropic efficiency of Tandem rotor stage under clean, radially hub distorted and radially tip distorted inflow conditions. After $\varphi = 0.67$, efficiency drops significantly under the hub distortion case. Around 10% of the drop in isentropic efficiency is observed in the case of radially hub distortion in comparison with clean inlet flow condition at $\varphi = 0.64$.

Figure 21 shows the performance map of Tandem rotor stage under clean flow, radially hub distorted flow and radially tip distorted flow. Tandem stage experiences a drop in total pressure and stall margin under radial distortion. In the case of radially hub distortion, maximum losses are observed at a different mass flow rate. At the

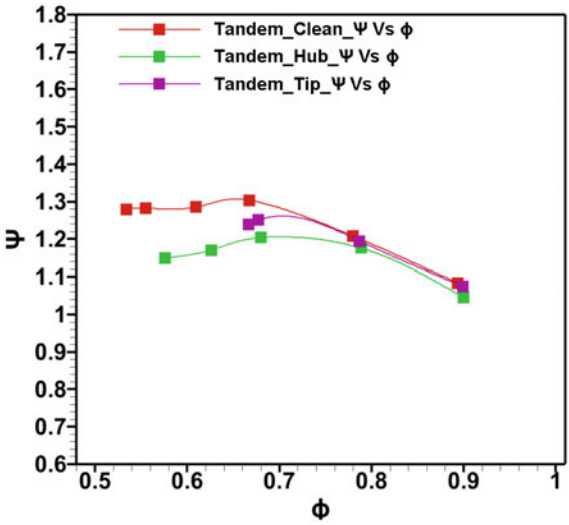

Fig. 21 Total pressure rise coefficient versus flow coefficient (φ) for tandem rotor

design mass flow rate, the tandem stage exhibits a drop of 6.55% in total pressure rise under radial hub distortion. In the case of radially tip distorted inflow, the stall range is largely affected. Tandem stage sees a drop off around 3% in the stall margin under hub distorted inflow. In the case of radial tip distortion, a sudden stall is observed.

5 Conclusion

The paper analyzes the effect of radial hub distorted and radial tip distorted inflow condition on the performance of tandem rotor stage in comparison with clean inlet flow condition. The paper also compares the performance of tandem rotor stage with baseline stage for different inlet flow condition. Various key findings from the present study are

1. At design point, tandem stage achieved higher total pressure rise and higher efficiency in comparison with the baseline stage at different inflow conditions. In comparison with single blade, higher diffusion factor can be achieved with the help of tandem blade.
2. In comparison with tandem stage, better stall margin is observed for the baseline stage. Performance of both stages drop substantially under radial distorted inflow.
3. Due to the low hub to tip design and higher flow turning, tandem stage experiences a substantial drop in a total pressure rise and isentropic efficiency under hub distorted inflow. In case of hub distorted inflow, migration of higher mass flow toward the tip region results in drop of the stall margin in comparison with the clean flow.
4. The stall margin of Tandem rotor stage under a clean flow inlet condition is 20%. In comparison with baseline stage drop of around 13% is observed in the stall margin of the Tandem rotor stage under clean inlet flow condition. Tandem rotor stage stall margin drops by 3% in case of radial hub distorted inflow condition in comparison with clean inlet flow condition. Both stages experience a drop in stall margin under tip distorted inflow. However, the effect of tip distorted region is more pronounced on the tandem rotor, where stall margin drops to 2% under tip distortion. A sudden stall is observed under tip distortion, which is attributed to the highly loaded tip design of the tandem rotor.
5. In case of the tandem rotor, strong tip leakage vortices from both forward and aft blade create a large blockage region. Further, wakes emanating from the forward and the aft blade mix with the tip leakage flow and result in a large flow blockage area under radial tip distortion, which leads to sudden stall.
6. The tandem blade needs to be designed with lower blade loading near the tip region. The strength of TLV can be further reduced by reducing the tip gap size. This will improve the performance of tandem blade near tip region, which will further help in improvising the stall margin.

References

1. Saha UK, Roy B (1997) Experimental investigation on tandem compressor cascade performance at low speeds. In: Experimental thermal and fluid science. Elsevier Inc
2. Falla G A C (2004) Numerical investigation of the flow in tandem compressor cascades. Diploma thesis, Universidad Nacional de Colombia, written at Institute of Thermal Powerplants, Vienna University of Technology
3. McGlumphy J, Ng W, Wellborn S, Kempf S (2007) Numerical investigation of tandem airfoils for subsonic axial-flow compressor blades. In: ASME Paper IMECE2007-43929, accepted for ASME J Turbomach
4. McGlumphy J, Ng W, Wellborn S, Kempf S (2008) 3-D numerical investigation of tandem airfoils for a core compressor rotor. In: Proceedings of ASME turbo expo, Berlin, Germany, 9–13 June 2008
5. Hasegawa H, Matsuoka A, Suga S (2003) Development of highly loaded fan with tandem cascade. In: AIAA paper 2003-1065
6. Linnemann H (1964) UntersuchungeneineseinstufigenAxialgelblasesmitTandemgittern, Konstruuktion, Heft 4, S 128
7. Brent JA, Clemmons DR (1974) Single-stage experimental evaluation of tandem airfoil rotor and stator blading for compressors. NASA CR-134713
8. Bammert K, Staude R (1979) Optimization for rotor blades of tandem design for axial flow compressors. In: ASME paper 79-GT-125
9. Weber A, Steinert W (1997) Design, optimization, and analysis of a high-turning transonic tandem compressor cascade. In: ASME 1997 international gas turbine and aeroengine congress and exhibition. American Society of Mechanical Engineers
10. Lee K-J, Lee B-H, Kang S-H, Jung J-H, Yang S-S, Lee D-S, Kwak J-S (2007) Development of block type inlet distortion simulating device for gas turbine engine inlet distortion test. Int J Aeronaut Space Sci 8:121125. https://doi.org/10.5139/IJASS.2007.8.2.121
11. Lee K, Lee B, Kang S, Yang S, Lee D (2010) Inlet distortion test with gas turbine engine in the altitude engine test facility. In: AIAA paper, 4337. https://doi.org/10.2514/6.2010-4337
12. Liu K, Sun Y, Zhong Y, Zhang H, Zhang K, Yang H (2014) Numerical investigation on engine inlet distortion under crosswind for a commercial transport aircraft. In: 29th congress of the International Council of the Aeronautical Sciences, St. Petersburg, Russia
13. Kumar A, Pradeep AM (2019) Design and off-design behaviour of a tandem rotor stage. In: Proceedings of IMechE (accepted for publication), Part G J Aerosp Eng